# Dynamic cofilin phosphorylation in the control of lamellipodial actin homeostasis

**Eleonora Jovceva[1], Martin R. Larsen[2], Michael D. Waterfield[1], Buzz Baum[1],* and John F. Timms[1,3]**

[1]Ludwig Institute for Cancer Research, UCL Branch, London, W1W 7BS, UK
[2]Department of Biochemistry and Molecular Biology, University of Southern Denmark, DK-5230 Odense, Denmark
[3]Translational Research Laboratory, Institute of Women's Health, University College London, London, WC1E 6DH, UK
*Author for correspondence (e-mail: b.baum@ucl.ac.uk)

## Summary

During animal cell chemotaxis, signalling at the plasma membrane induces actin polymerisation to drive forward cell movement. Since the cellular pool of actin is limited, efficient protrusion formation also requires the coordinated disassembly of pre-existing actin filaments. To search for proteins that can monitor filamentous and globular actin levels to maintain the balance of polymerisation and disassembly, we followed changes in the proteome induced by RNA interference (RNAi)-mediated alterations in actin signalling. This unbiased approach revealed an increase in the levels of an inactive, phosphorylated form of the actin-severing protein cofilin in cells unable to generate actin-based lamellipodia. Conversely, an increase in F-actin levels induced the dephosphorylation and activation of cofilin via activation of the Ssh phosphatase. Similarly, in the context of acute phosphoinositide 3-kinase (PI3K) signalling, dynamic changes in cofilin phosphorylation were found to depend on the Ssh phosphatase and on changes in lamellipodial F-actin. These results indicate that changes in the extent of cofilin phosphorylation are regulated by Ssh in response to changes in the levels and/or organisation of F-actin. Together with the recent finding that Ssh phosphatase activity is augmented by F-actin binding, these results identify Ssh-dependent regulation of phosphorylated cofilin levels as an important feedback control mechanism that maintains actin filament homeostasis during actin signalling.

## Introduction

Animal cells respond to a variety of signalling events at the plasma membrane by remodelling their actin cytoskeleton (Ridley et al., 2003). This drives changes in cell shape and is important for a variety of morphogenetic events, including cell migration and axon pathfinding. In many of these systems, actin signalling is triggered by ligand-receptor binding at the outer leaflet of the plasma membrane. This induces the activation of intracellular phosphoinositide 3-kinase (PI3K), which leads to the local activation of Rho family GTPases (Katso et al., 2001; Vanhaesebroeck et al., 2001). Rho family GTPases serve as 'master regulators' of the actin cytoskeleton (Ridley et al., 2003). Once active and loaded with GTP, Cdc42 and Rac GTPases bind Arp2/3 activator complexes, WASp and SCAR, respectively (Ibarra et al., 2005; Vartiainen and Machesky, 2004), triggering the Arp2/3-dependent nucleation of actin filaments and the generation of local actin-dependent protrusions. Since the burst of actin polymerisation in response to signalling is limited by the availability of actin monomers, a robust protrusive response also requires the coincident disassembly of the existing actin network. This is catalysed by the conserved actin-binding protein cofilin (Bamburg, 1999; Carlier et al., 1997; Hotulainen et al., 2005; Nishita et al., 2005) For a robust chemotactic response, the turnover of newly formed actin-based protrusions must also be tightly regulated, so that a cell can follow dynamic changes in the direction of an extracellular gradient. Finally, it has been proposed that cofilin aids directional motility by severing actin filaments close to the cell front to create new barbed ends to promote new local actin polymerisation (Ghosh et al., 2004).

Although data from the literature suggest that Rho family GTPases help to achieve coordinated control of actin filament nucleation and disassembly (Arber et al., 1998; Yang et al., 1998), little is known about the molecular mechanisms that monitor changes in actin organisation to ensure that a protrusive response to signalling is robust and self-limiting. To identify cytoskeletal regulators that function in this way, we used 2D difference gel electrophoresis (2D-DIGE) together with RNA interference (RNAi) to search for protein isoforms that are sensitive to changes in actin filament organisation and to actin signalling in *Drosophila* S2R^{+} cells. This identified Ssh-dependent changes in cofilin phosphorylation that mirror changes in actin filament levels. Taken together, our data suggest that the dynamic regulation of cofilin activity acts as a feedback control mechanism, which monitors the level of actin filaments and helps to restore the resting state of the cytoskeleton following acute signalling.

## Results

### Levels of phosphorylated cofilin change in response to changes in actin filament organisation and PI3K signalling

The ability of animal cells to control and coordinate cortical actin-filament-based protrusive activity, suggests the existence of cellular machinery that monitors and regulates actin filament levels. To explore this possibility, we took an unbiased approach, using 2D-DIGE to search for protein isoforms that are sensitive to RNAi-induced changes in actin cytoskeleton organisation. We chose *Drosophila* S2R$^+$ cells, an adherent isolate of the commonly used haemocyte-derived S2 cell line (Yanagawa et al., 1998), as a model system for this analysis. Triplicate cultures were treated with double-stranded RNA (dsRNA) to silence genes that affect lamellipodial formation (Kunda et al., 2003); 2D-DIGE was performed to identify corresponding changes in the S2R$^+$ proteome, taking advantage of the fact that cytoskeletal proteins are relatively abundant in S2R$^+$ extracts. Protein expression was first assayed in lysates from untreated control cells and from cells treated with dsRNAs targeting Cdc42, Rac1+Rac2 and Arp3 prepared on different days. These treatments all eliminate lamellipodial formation (Kunda et al., 2003). This analysis revealed a number of proteins whose expression differed between untreated control and one or more of the experimental conditions (>1.5-fold average up- or downregulation; $P<0.05$; $n$=3). Each of these protein spots was excised from the gels for mass spectrometry (MS)-based protein identification (supplementary material Table S1). In this way, a protein corresponding to *Drosophila* Twinstar – the homologue of the actin depolymerising and severing protein cofilin – was identified with high confidence. This cofilin isoform was expressed at elevated levels following loss of Cdc42, Rac and Arp3 expression (Fig. 1A, B and supplementary material Fig. S1).

Cdc42 and Rac have been implicated in the dynamic regulation of cofilin activity in several systems (Arber et al., 1998; Yang et al., 1998) and are thought to act as part of a PI3K signalling cascade (Benard et al., 1999; Hawkins et al., 1995; Kotani et al., 1995; Reif et al., 1996). These facts led us to use RNAi to explore whether PI3K signalling also influences the expression of this cofilin isoform in S2R$^+$ cells. To do this, we treated cells with dsRNAs targeting *Drosophila* PI3K or the phosphatidylinositol (3,4,5)-trisphosphate [PtdIns(3,4,5)$P_3$] phosphatase PTEN to perturb PtdIns(3,4,5)$P_3$ levels in opposing directions. In addition, we used RNAi to silence two crucial downstream targets of PI3K signalling, Akt and Ras. GFP dsRNA was included as an irrelevant control for the effects of RNAi. A quantitative analysis revealed a significant reduction in the level of this cofilin spot in PTEN dsRNA-treated cells (–1.57-fold; $P$=0.005) and a moderate upregulation in PI3K dsRNA-treated cells, as expected for a genuine target of PI3K signalling (Fig. 1 and supplementary material Table S1). The decrease in the level of this cofilin isoform observed in Akt RNAi cells fell below our confidence limit (Fig. 1B,C). As expected, GFP dsRNA treatment did
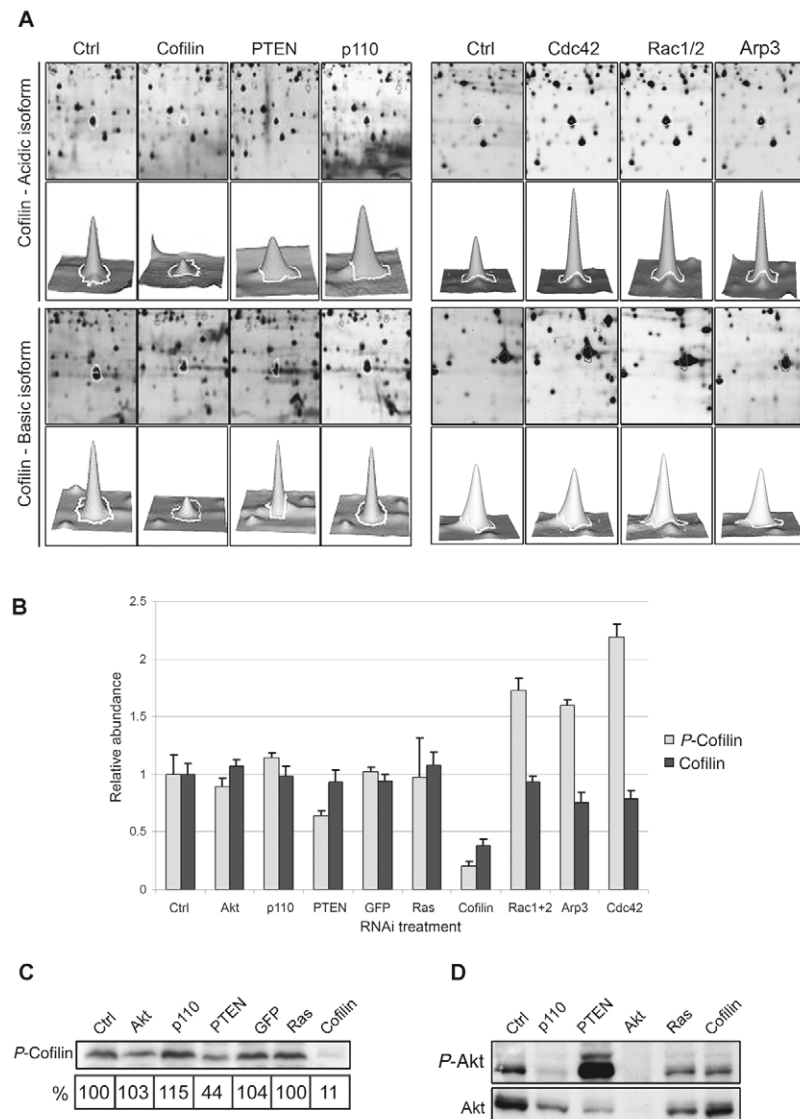


Fig. 1. *P*-cofilin levels change in response to alterations in actin filament organisation and PI3K signalling. (A) Representative 2D-DIGE gel images and 3D-fluorescence profiles of acidic and basic cofilin isoforms are shown for untreated (Ctrl) cells and cells treated with control dsRNA and dsRNA targeting cofilin, PTEN, PI3K p110 catalytic subunit (p110), Cdc42, Rac1 and Rac2 (Rac1/2), and Arp3. (B) The relative abundances of *P*-cofilin (acidic isoform) and cofilin (basic isoform) are shown for RNAi-treated cells from 2D-DIGE image analysis. Values represent the average of three measurements from biological replicates. Error bars represent the standard deviation. (C) Immunoblots show *P*-cofilin levels in untreated control and dsRNA-treated S2R$^+$ cell lysates confirming 2D-DIGE data. Relative abundance is shown below the blot as a percentage of the control, and is the average calculated from densitometry measurements of blots from three independent experiments. (D) Immunoblot of *P*-Akt and total Akt levels in control and dsRNA-treated S2R$^+$ cell lysates confirms the loss of PI3K, PTEN and Akt expression.

not affect cofilin expression. Nevertheless, one protein, identified as annexin B11, exhibited significant differences in its expression between dsRNA-treated cells and the untreated control. This suggests that dsRNA treatment or the engagement of the RNAi machinery itself can alter the expression of some proteins even in the absence of a target mRNA.

A second more basic isoform of cofilin was identified on these 2D gels by matrix-assisted laser desorption/ionization time-of-flight (MALDI-TOF)-based peptide mass fingerprinting (supplementary material Fig. S1A), and the identification of both isoforms was confirmed by the concomitant reduction of both the basic and acidic gel features in cofilin RNAi-treated cells (supplementary material Table S1 and Fig. 1C,D). Based on previous 2D studies (de Graauw et al., 2005; Hensbergen et al., 2005), we reasoned that the acidic isoform of cofilin may be phosphorylated. To test whether this was indeed the case, $TiO_2$ micro-columns were used to enrich for tryptic phosphopeptides from the acidic cofilin gel feature, which were then subjected to MALDI-TOF analysis. This identified a peptide with a mass corresponding to a phosphorylated form of the N-terminal tryptic peptide of cofilin (Ac-ASGVTVSDVCK+$P$; 1244.5 Da), with the equivalent peptides from the acidic and basic gel features exhibiting an 80 Da mass difference, equal to the mass of one phosphate group (supplementary material Fig. S1C). Nano-liquid chromatography-electrospray ionization collision-induced dissociation tandem mass spectrometry (LC-MS/MS)-based sequencing was used to identify the site of phosphorylation as being serine residue 3 (supplementary material Fig. S2). Significantly, this modification is known to block the activity of cofilin by preventing it from binding to and severing actin filaments (Bamburg, 1999). Since commercially available antibodies raised against cofilin phosphorylated at Ser3 (hereafter referred to as $P$-cofilin) did not recognise the *Drosophila* protein, a rabbit polyclonal antibody was raised against the *Drosophila* phospho-peptide sequence. The affinity-purified antibody specifically recognised the acidic isoform of cofilin in 2D immunoblots (supplementary material Fig. S1D), again confirming the identity of this protein. This antibody against $P$-cofilin was then used to validate the results of the proteomic analysis by immunoblotting lysates of the dsRNA-treated cells (Fig. 1C). Antibodies against Akt phosphorylated at Ser505 ($P$-Akt) and against total Akt were used in a similar way to demonstrate the efficacy of the PI3K, PTEN and Akt RNAi treatments (Fig. 1D). Taken together, these data show that the extent of cofilin phosphorylation is responsive to changes in PtdIns(3,4,5)$P_3$ levels and is dependent on the activity of Cdc42 and Rac. More surprisingly, these results also indicate that cofilin phosphorylation is affected by changes in the level of Arp3, a component of the actin nucleation complex that drives lamellipodial formation downstream of Cdc42 and Rac (Kunda et al., 2003).

### Kinetics of cofilin phosphorylation and actin remodelling in response to an acute stimulus

Having identified changes in the extent of cofilin phosphorylation in cells at steady state, we next examined the dynamics of cofilin phosphorylation in cells undergoing acute changes in actin cytoskeletal organisation. This required the identification of a stimulus able to induce dynamic actin

remodelling. In testing a number of growth factors in S2R$^+$ cells [10% foetal calf serum (FCS), 2-day-old conditioned medium, bovine insulin, human EGF, murine vascular endothelial growth factor (VEGF) and human platelet-derived growth factor (PDGF)], only insulin was found to activate signalling, as monitored by immunoblotting with specific antibodies against $P$-Akt, S6K phosphorylated at Thr398 ($P$-S6K) and ERK phosphorylated at Thr198 and Tyr200 ($PP$-ERK) (supplementary material Fig. S3A) and Lizcano et al. (Lizcano et al., 2003). Insulin also induced an increase in the level of lamellipodial F-actin in these cells within 5 minutes of treatment (Fig. 2A). Elevated levels of filamentous actin remained at the cell cortex for 30-40 minutes, before moving to the cell interior (perhaps as the result of retrograde flow in the absence of new polymerisation). Since actin polymerisation is known to generate the force for membrane protrusion, we used time-lapse microscopy to determine whether this burst of actin filament formation is translated into protrusive activity, imaging cells every 20 seconds before and after addition of insulin, starting 10 minutes before and finishing 30 minutes after addition. (Fig. 2B). As can be seen in the corresponding kymographs, insulin induced a significant increase in the rate of membrane ruffling. Insulin was also found to induce strong cortical F-actin staining in more rounded Kc167 cells, which do not possess lamellipodia (Fig. 2C). This suggests that the induction of actin polymerisation is the primary response, which in adherent S2R$^+$ cells is translated into the formation of F-actin-based protrusions.

The kinetics of this actin response was mirrored by changes in PI3K signalling, as measured using $P$-Akt. The insulin-induced change in Akt phosphorylation reached its maximum level within 2 minutes. High levels of $P$-Akt were then maintained for 10-20 minutes, before declining gradually to background levels (Fig. 2E). This kinetic profile was confirmed in fixed cells where, in response to insulin, $P$-Akt was first seen to rapidly accumulate at the plasma membrane, the site of PtdIns(3,4,5)$P_3$ generation (supplementary material Fig. S3B). $P$-Akt then became localised to the nucleus, before declining to barely detectable levels by 120 minutes. We confirmed this to be a generic response of fly cells by observing similar $P$-Akt dynamics in Kc167 cells following insulin stimulation (supplementary material Fig. S3C). We then used immunoblotting to follow cofilin phosphorylation dynamics during the course of this response. $P$-cofilin levels responded to PI3K signalling, but did not peak until ~30 minutes after insulin stimulation (Fig. 2D); long after the initial burst of actin and PI3K signalling.

Having established that insulin induces a robust PI3K signal together with a striking change in actin organisation and cofilin phosphorylation, we used the PI3K inhibitors LY294002 and wortmannin to test whether these events are causally linked. The addition of LY294002 (100 $\mu$M) or wortmannin (100 nM) to resting S2R$^+$ cells (Fig. 3A) and Kc167 cells (supplementary material Fig. S4A) led to a profound loss of cortical actin filaments. Moreover, both inhibitors blocked normal membrane ruffling in cells (Fig. 3B), suggesting a role for PtdIns(3,4,5)$P_3$ in the regulation of actin dynamics in cells at steady state. In addition, LY294002 and wortmannin induced a retraction of the cell edge, leaving a few relatively inactive membrane processes attached to the substrate. Similarly, both drugs blocked the ruffling response to insulin treatment

(supplementary material Fig. S4B). The ability of these compounds to block insulin-induced PI3K activity was confirmed by immunoblotting for *P*-Akt (Fig. 3C). We were then able to use LY294002 to show that insulin-stimulated cofilin phosphorylation is a consequence of PI3K signalling itself, because treatment with this compound led to a significant reduction in the ability of insulin to induce cofilin phosphorylation (Fig. 3D). Thus, PtdIns(3,4,5)$P_3$ is required
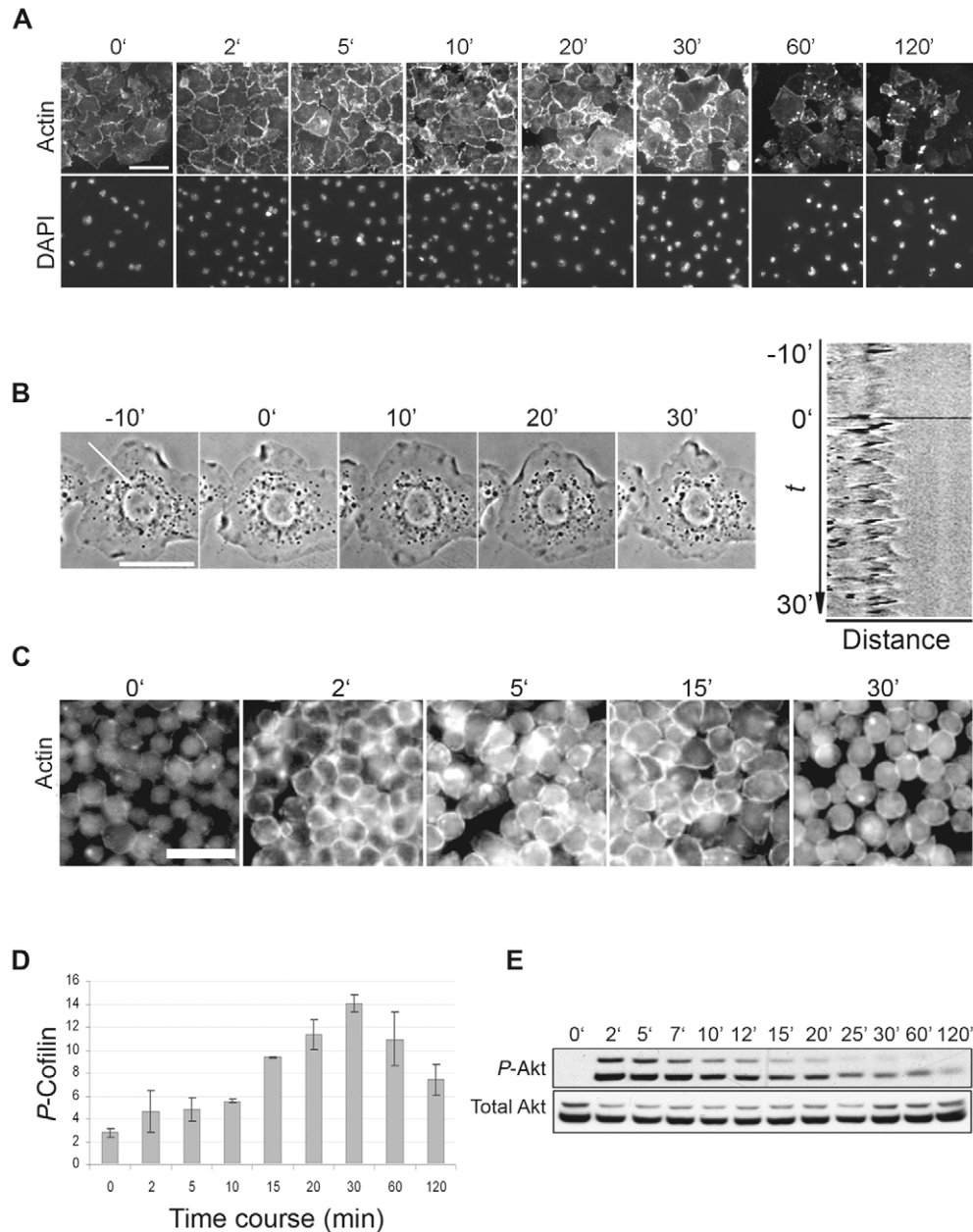
**Fig. 2.** The kinetics of actin remodelling and cofilin phosphorylation following an acute stimulus. (A) S2R$^+$ cells stained for F-actin (Rhodamine-phalloidin) and nuclei (DAPI) are shown at various times after insulin stimulation (10 $\mu$g/ml). Bar, 50 $\mu$m. (B) Images from a time-lapse movie of S2R$^+$ cells stimulated with insulin (10 $\mu$g/ml) for the times indicated. Cells were filmed in phase-contrast on a time-lapse microscope using a 100$\times$ oil-immersion lens; frames were acquired every 20 seconds, 10 minutes prior to insulin addition and for 30 minutes after addition. Images are representative of five independent experiments. Bar, 50 $\mu$m. Right panel shows a kymograph of the movie from which the presented images were taken, generated from pixel intensities along a line transecting the cell membrane (shown in first image). It shows increased protrusion dynamics after insulin stimulation. (C) F-actin immunostaining (Rhodamine-phalloidin) of serum-starved Kc167 cells stimulated with insulin (10 $\mu$g/ml) for the indicated times. Bar, 50 $\mu$m. (D) Cofilin is transiently phosphorylated in S2R$^+$ cells in response to insulin. S2R$^+$ cells were grown in serum-free medium overnight and stimulated with insulin at 10 $\mu$g/ml for the indicated times. Lysates were prepared and immunoblotted with antibody against *P*-cofilin. Blots were analysed by densitometry. Values represent the mean *P*-cofilin signal from two experiments after normalising with respect to $\beta$-actin levels. Error bars represent the standard deviation. (E) Time course of Akt activation in insulin stimulated S2R$^+$ cells. S2R$^+$ cells were maintained in Schneider's serum-free medium overnight, and then stimulated with bovine insulin (10 $\mu$g/ml) for the times indicated. Immunoblotting was used to assess levels of *P*-Akt and total Akt.

for the maintenance of an actin-rich cortex, the normal ruffling behaviour of resting cells, and for the insulin-induced stimulation of actin polymerisation and cofilin phosphorylation in S2R$^+$ cells.

## Functional analysis of cofilin and *P*-cofilin during acute actin signalling

Using RNAi, we were then able to define roles for cofilin and phosphorylated cofilin (*P*-cofilin) in the response of S2R$^+$ cells to PI3K signalling. As before, insulin was used to stimulate PI3K-dependent membrane ruffling (Fig. 4). We first tested the role of cofilin in this process. Five days after the treatment of cells with cofilin dsRNA, the majority of cells (>90%) displayed a rounded morphology, with increased F-actin staining (Fig. 4A). These cells were unable to re-organise their actin cytoskeleton or to ruffle in response to insulin (Fig. 4B), implying a role for cofilin in the generation of new actin filaments, as previously described (Ghosh et al., 2004). Second, since the kinase and phosphatase responsible for the control of cofilin phosphorylation have been previously identified in both *Drosophila* and other systems, as LIMK (Arber et al., 1998; Yang et al., 1998) and slingshot (Ssh) (Niwa et al., 2002), respectively, we were able to use RNAi to assess whether the dynamic changes in cofilin phosphorylation observed are dependent on these proteins and important for the protrusive response to PI3K signalling. As expected, RNAi-induced silencing of Ssh led to an increase in basal cofilin phosphorylation, whereas silencing of LIMK led to a decrease (Fig. 5A). Ssh silencing also induced a significant reduction in the ability of cells to mount a protrusive response to insulin stimulation (Fig. 4B), even though gross cellular morphology and actin organisation were preserved (Fig. 4A). Conversely, cells expressing reduced levels of LIMK were found to have well-defined cortical lamella (Fig. 4A) and to ruffle intensely before and after insulin stimulation (Fig. 4B), suggesting that cofilin phosphorylation is not required for the formation of new protrusions. Finally, we used RNAi to test for the role of Rac and the Arp2/3 complex in this response. As previously reported (Kunda et al., 2003), dsRNAs targeting Rac1+2 or Arp3 gave rise to S2R$^+$ cells with a starfish-like phenotype. These cells proved unable to mount a morphological response to insulin treatment (Fig. 4A,B). Thus, the Rac-Arp2/3 pathway is required for the generation of new actin filament-based protrusions downstream of acute PI3K signalling, as is active cofilin.

## Actin filaments control cofilin phosphorylation dynamics

The proteomic analysis showed that cells lacking lamellipodia (Rac1/2, Cdc42 or Arp3 RNAi cells) express relatively high levels of *P*-cofilin (Fig. 1). This suggested the possibility that the observed changes in cofilin phosphorylation are triggered as a response to the loss of
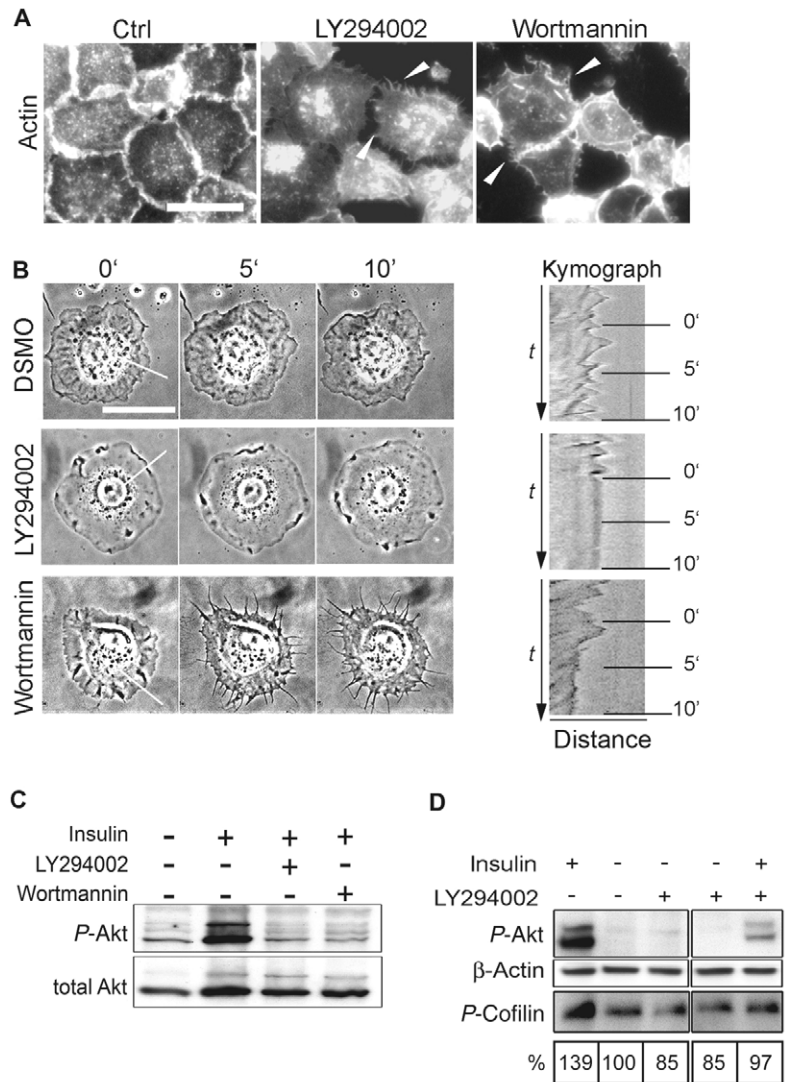


**Fig. 3.** PI3K-signalling controls cortical actin organisation. (A) Actin staining of S2R$^+$ cells after treatment with DMSO vehicle (Ctrl), LY294002 (100 μM) and wortmannin (100 nM). Cells were treated for 10 minutes and then fixed and stained with Rhodamine-phalloidin. Arrowheads indicate regions of cell retraction to leave protrusions. Bar, 50 μm. (B) Images of time-lapse movies of S2R$^+$ cells treated with DMSO, LY294002 (100 μM) and wortmannin (100 nM). Cells were filmed in phase-contrast on a time-lapse microscope using a 100× oil-immersion lens. Frames were acquired every 10 seconds for 30 minutes with inhibitor treatment after 10 minutes of filming (designated 0' in the figure). Snapshots are shown at 0, 5 and 10 minutes. The corresponding kymographs show cells from 3 minutes before until 10 minutes after insulin stimulation and were constructed from pixel intensities taken along the lines depicted in the images on the left. Bar, 50 μm. (C) Immunoblotting of *P*-Akt and total Akt in untreated S2R$^+$ cells and cells treated with insulin (for 10 minutes) with and without pre-treatment (for 10 minutes) with LY294002 (100 μM) or wortmannin (100 nM). (D) Immunoblotting of *P*-Akt, β-actin and *P*-cofilin in S2R$^+$ cells treated for 10 minutes with LY294002 (100 μM) and insulin (10 μg/ml), alone and in combination. Relative abundance is represented as a percentage of the control below the blot and is the average calculated from densitometry measurements of blots from three independent experiments.

lamellipodial actin. To test whether this correlation also holds during an acute response to PI3K signalling, we used Rac1 + Rac2 RNAi to block lamellipodial formation in cells stimulated

with insulin. This RNAi treatment eliminated dynamic changes *P*-cofilin, supporting the idea that changes in cofilin activity follow changes in the levels of actin filaments in this system (Fig. 5B). Similarly, Ssh RNAi cells, which have an impaired ruffling response, do not display the dynamic changes in cofilin phosphorylation in response to insulin/PI3K signalling (Fig. 5B). To examine the kinetics of this response more directly, we used actin inhibitors to induce acute changes in the relative levels of F-actin and G-actin, and tracked the resulting changes in *P*-cofilin levels. Both the G-actin-sequestering agent latrunculin B and the barbed-end capping toxin cytochalasin D eliminated the actin-rich cell cortex within minutes (Kiger et al., 2003) (data

not shown). In both cases, this led to a steady increase in the level of cofilin phosphorylation over a period of 30-60 minutes (Fig. 5C). Conversely, the addition to cells of jasplakinolide, a drug that promotes actin filament formation (Bubb et al., 1994), induced the rapid loss of *P*-cofilin (to barely detectable levels within 10 minutes). Jasplakinolide was also able to block the accumulation of *P*-cofilin in insulin-treated cells (Fig. 5D). These data reveal a direct correlation between the level of cortical actin filaments present in cells and the level of cofilin phosphorylation.

RNAi-induced silencing of actin was also found to induce a robust increase in cofilin phosphorylation (Fig. 6D). This confirms the link between actin filaments and *P*-cofilin, and shows that free cofilin can serve as a substrate for LIMK. Importantly, it also demonstrates that G-actin is not required for a change in F-actin or G-actin levels to be translated into a change in the extent of cofilin phosphorylation. Actin-dependent changes in cofilin phosphorylation could be mediated through changes in the rate of its phosphorylation and/or its dephosphorylation. To explore both possibilities, we used LIMK and Ssh dsRNA to reduce the rate of both forward and back reactions. This analysis revealed first that the loss of *P*-cofilin observed following the treatment of cells with jasplakinolide requires Ssh (Fig. 6A). This loss of the jasplakinolide response was not due to the raised levels of phosphorylated Ser3 in Ssh RNAi cells, because Ssh dsRNA also blocked the jasplakinolide-induced decrease in *P*-cofilin levels in cells lacking both Ssh and LIMK (Fig. 6B). By contrast, although RNAi-induced silencing of LIMK significantly reduced the overall levels of *P*-cofilin, it was unable to suppress changes in *P*-cofilin levels seen upon treatment of cells with latrunculin (Fig. 6C). Significantly, however, the addition of Ssh dsRNA to LIMK RNAi cells overrode this latrunculin-induced increase in *P*-cofilin levels. These results suggest that the downregulation of Ssh phosphatase activity after latrunculin treatment plays an important role in the regulation of the *P*-cofilin response, as does its upregulation in the presence of jasplakinolide. Thus, Ssh is likely to be the key regulator of dynamic regulation of cofilin phosphorylation this system.
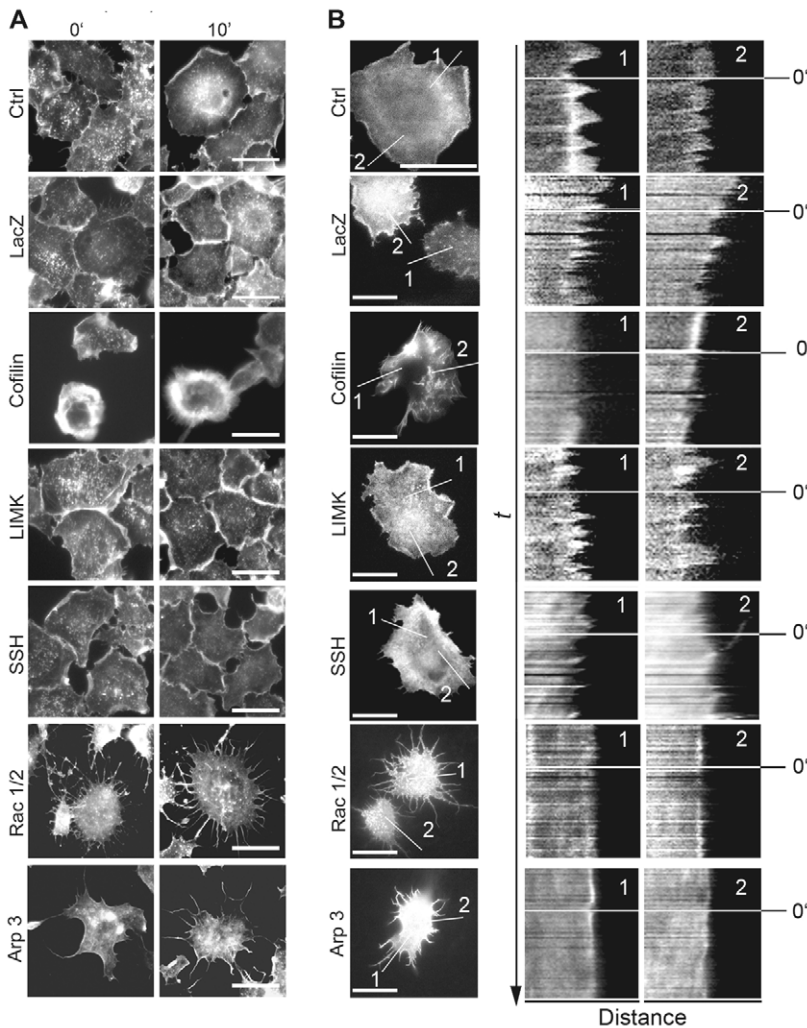
## Discussion

In this study, we have used *Drosophila* cell lines as a model system to explore the molecular mechanisms governing the dynamic remodelling of the cortical actin cytoskeleton. First, we sought to identify mechanisms that enable cells to sense and respond to changes in actin filament levels. To do this, we took an unbiased approach, making use of the relative abundance of cytoskeletal regulators to combine proteome expression profiling with RNAi-dependent gene silencing to identify proteins that are responsive



**Fig. 4.** Functional analysis of cofilin during acute actin signalling. (A) Actin staining in dsRNA-treated cells stimulated with insulin. S2R$^+$ cells were incubated with dsRNAs targeting LacZ, cofilin, LIMK, Ssh, Rac1and Rac2 (Rac1/2) and Arp3 for 5 days. On day 5, cells were treated with insulin for 10 minutes (10') or left untreated (0'). Cells were then fixed and stained for F-actin with Rhodamine-phalloidin. Bars, 50 μm. (B) Visualisation of actin dynamics in dsRNA-treated cells using GFP-labelled moesin. Snapshots of time-lapse movies just before the addition of insulin are shown on the left. Bars, 50 μm. The two lines used to generate the kymographs (right) are indicated on the cell images. Actin reorganisation was filmed for 3 minutes before and for 10 minutes after the addition of 10 μg/ml insulin, the point of insulin addition labelled as 0'. Images are representative of at least two independent experiments.
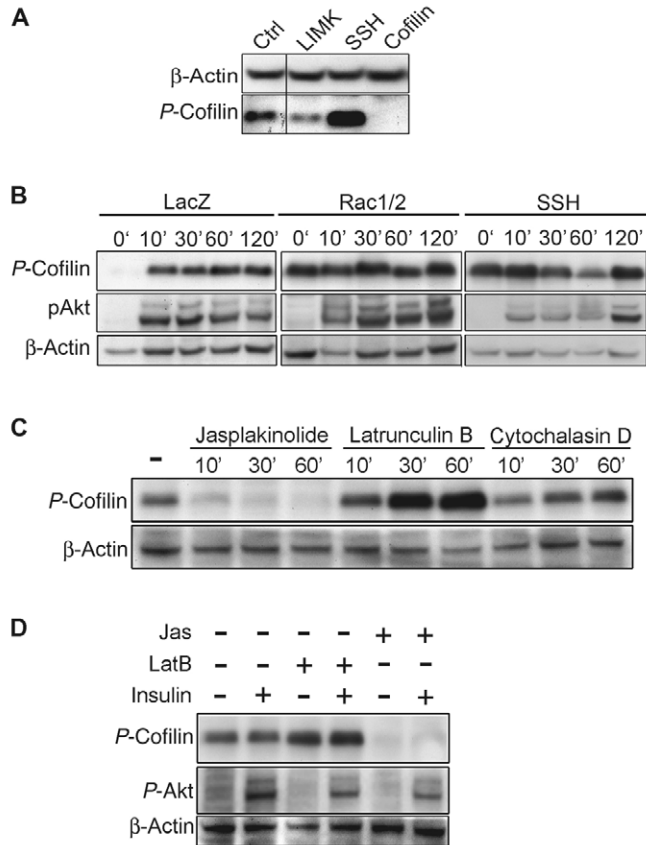
**A**



**B**



**C**



**D**



**Fig. 5.** PI3K-induced changes in cofilin phosphorylation are the result of actin cytoskeletal remodelling. (A) LIMK and Ssh are regulators of cofilin phosphorylation. S2R^{+} cells were left untreated (Ctrl) or were treated with dsRNA for knockdown of expression of LIMK, Ssh and cofilin for 5 days. Cells were lysed and *P*-cofilin and β-actin levels assessed in the lysates by immunoblotting. (B) Immunoblotting of *P*-cofilin, *P*-Akt and β-actin in lysates of dsRNA-treated cells stimulated with insulin. S2R^{+} cells were cultured in the presence of dsRNA targeting LacZ (control), Rac1+2 and Ssh and then treated with 10 µg/ml insulin for the indicated times prior to lysis and immunoblotting. (C) *P*-cofilin and β-actin levels were assessed in extracts from S2R^{+} cells treated with jasplakinolide (1 µg/ml), latrunculin B (1 µg/ml) or cytochalasin D (2 µg/ml) for the times indicated. (D) *P*-cofilin, *P*-Akt and β-actin levels are shown for S2R^{+} cells pre-treated for 10 minutes with latrunculin B (1 µg/ml) or jasplakinolide (1 µg/ml) followed by 20 minutes of insulin treatment (10 µg/ml) or vehicle alone.
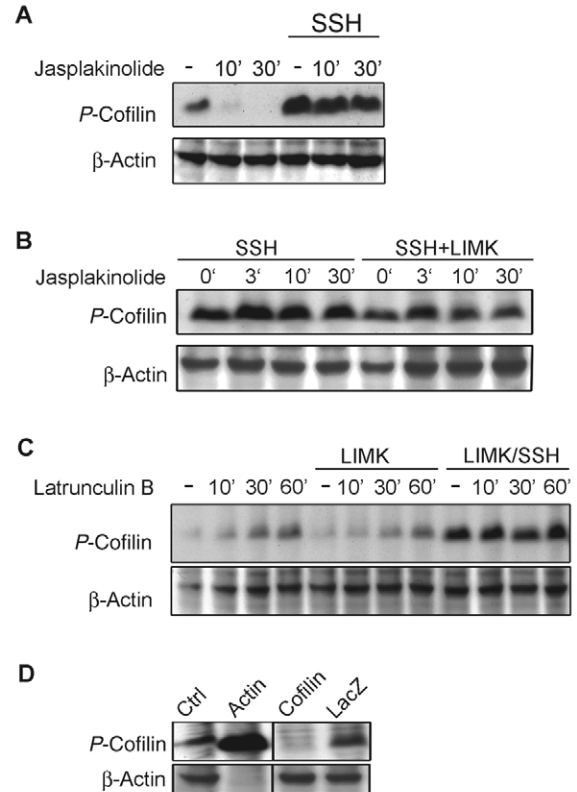
**A**



**B**



**C**



**D**



**Fig. 6.** Slingshot is the major regulator of actin-dependent cofilin phosphorylation. (A) Ssh RNAi blocks jasplakinolide-induced loss of cofilin phosphorylation. Control S2R^{+} cells and cells treated with dsRNA targeting Ssh were treated with jasplakinolide (1 µg/ml) for the times indicated and *P*-cofilin and β-actin levels assessed in the lysates by immunoblotting. (B) LIMK RNAi does not reverse Ssh dsRNA blockade of jasplakinolide-induced loss of cofilin phosphorylation. Cells treated with dsRNA targeting Ssh (SSH) or Ssh and LIMK together (SSH/LIMK) were treated with jasplakinolide (1 µg/ml) for the indicated times, and *P*-cofilin and β-actin levels assessed in lysates by immunoblotting. (C) The effect of LIMK and Ssh on latrunculin B-induced cofilin-phosphorylation. Cells treated with control dsRNA and dsRNA targeting LIMK or LIMK and SSH together (LIMK/SSH) were treated with latrunculin B (1 µg/ml) for the indicated times, and *P*-cofilin and β-actin levels in lysates were determined by immunoblotting. (D) Loss of actin expression induces cofilin phosphorylation. *P*-cofilin and β-actin levels were determined by immunoblotting in lysates of control cells (untreated) and cells treated with dsRNAs targeting actin, cofilin and LacZ.

to changes in lamellipodial actin organisation. *P*-cofilin was the only protein spot identified whose expression correlated with actin filament levels. Significantly, phosphorylation of cofilin on the evolutionarily conserved Ser3 prevents the binding of cofilin to actin filaments, completely inhibiting its ability to promote filament disassembly (Bamburg, 1999). *P*-cofilin levels were also altered in opposing directions in response to changes in levels of PtdIns(3,4,5)$P_3$ induced following PI3K and PTEN RNAi, but were unaffected by RNAi-induced silencing of Ras and Akt. Thus, the level of cofilin phosphorylation is responsive to changes in actin organisation and is regulated by actin-signalling events downstream of PtdIns(3,4,5)$P_3$ (Firtel and Chung, 2000).

Having established a possible link between PI3K-actin signalling and cofilin phosphorylation, we were then able to use RNAi together with live cell imaging to look for a role for the active dephosphorylated form of cofilin in actin remodelling. The ability of cells to mount a ruffling response in this system was found to require cofilin and, to a lesser extent, its dedicated phosphatase Ssh, in agreement with previous reports (Ghosh et al., 2004; Nishita et al., 2004). Moreover, levels of *P*-cofilin were found to respond to PI3K signalling, as has been observed in other systems (Mouneimne et al., 2004; Nishita et al., 2004). In S2R^{+} cells, *P*-cofilin levels peak 30 minutes after insulin stimulation before gradually returning to baseline levels. Although this dynamic response reveals a link between PI3K signalling and cofilin phosphorylation, as suggested by the analysis in steady state

(Fig. 4), three pieces of evidence indicated that the observed changes in cofilin phosphorylation status were unlikely to mediate PI3K-induced actin remodelling. First, PI3K signalling, cortical actin accumulation and membrane ruffling all occur within the first few seconds or minutes of insulin addition; before the detection of any significant changes in cofilin phosphorylation. Second, the morphogenetic response to insulin was unaffected by the loss of LIMK, the kinase responsible for cofilin phosphorylation in this and other systems (Fig. 4) (Arber et al., 1998; Yang et al., 1998), suggesting that an increase in cofilin phosphorylation is not required for cytoskeletal remodelling during the initial protrusive response. Third, it is clear from the literature that the relationship between PI3K-signalling and cofilin phosphorylation varies widely across the different systems in which it has been analysed (Mouneimne et al., 2004; Nishita et al., 2004; Song et al., 2006). These data led us to explore an alternative model in which changes in cofilin phosphorylation are a downstream effect of PI3K-induced changes in actin filament formation. The first indication that this might be the case came from the finding that in our 2D-DIGE analysis, $P$-cofilin levels were increased in Arp3 RNAi cells, in which lamellipodia and the underlying cortical actin network are lost (Biyasheva et al., 2004; Kunda et al., 2003). Second, in Rac RNAi cells, which are unable to generate protrusions, $P$-cofilin levels remained at a constant and elevated level following insulin stimulation – as expected by such a model. Third, the treatment of cells with latrunculin B or cytochalasin D caused the rapid loss of cortical F-actin, and a delayed increase in $P$-cofilin levels. Conversely, the actin toxin jasplakinolide induced ectopic actin filament formation and a relatively rapid and complete loss of the $P$-cofilin signal. Moreover, jasplakinolide also blocked the ability of insulin to induce cofilin phosphorylation in these cells. Taken together these data show that actin remodelling is required for dynamic changes in the level of cofilin Ser3 phosphorylation, and that acute changes in actin filaments levels are sufficient to alter the cofilin phosphorylation status.

It is noticeable that the increase in cofilin phosphorylation is observed in cells with a paucity of cortical actin filaments, where it will limit the rate of filament disassembly. Conversely, cofilin is dephosphorylated and activated in cells with excess actin filaments, therefore maintaining the monomeric actin pool. This suggests a role for the dynamic regulation of cofilin phosphorylation in the maintenance of actin filament homeostasis and implies the existence of a sensor that can measure dynamic changes in actin filament levels. Four recent studies have implicated Ssh in this role, by showing that Ssh is activated through binding to actin filaments (Nagata-Ohashi et al., 2004; Soosairajah et al., 2005; Tanaka et al., 2005; Yamamoto et al., 2006). Similarly, our data show that Ssh is likely to be the key regulator of $P$-cofilin levels in S2R$^+$ cells because it is required for dynamic changes in $P$-cofilin levels in response to insulin and because the kinetics of loss of cofilin phosphorylation following jasplakinolide treatment are more rapid than the effects of latrunculin B – as would be expected if the dynamics of $P$-cofilin were regulated by a constitutively active LIMK and a phosphatase whose activity is regulated by the level of actin filaments. Furthermore, Ssh RNAi suppresses both jasplakinolide- and latrunculin-induced changes in $P$-cofilin whereas, on its own, LIMK RNAi cannot. Because

RNAi-mediated silencing of actin mimics the effects of actin depolymerisation by increasing the level of cofilin phosphorylation, it is unlikely that G-actin levels play a significant role in driving the change in $P$-cofilin levels following a perturbation of the ratio between F-actin and G-actin. Instead, we favour a model in which the binding of Ssh to actin filaments acts as a measure of relative levels of F actin.

How can we reconcile the role of cofilin in the formation of actin-dependent protrusions in S2R$^+$ cells with the observed changes in $P$-cofilin following an acute PI3K response? We suggest the following scenario: following insulin addition, PI3K is activated within 2 minutes, inducing the conversion of phosphatidylinositol (4,5)-bisphosphate [PtdIns(4,5)$P_2$] to PtdIns(3,4,5)$P_3$ within the inner leaflet of the plasma membrane. This activates Rac, possibly through the association of an unidentified PH domain-containing Rac-GEF with PtdIns(3,4,5)$P_3$, leading to the nucleation of Arp2/3-dependent actin filaments at the cell cortex with subsequent filament elongation and protrusion formation. In these cells, active non-phosphorylated cofilin at the cell front will depolymerise existing ADP-actin filaments to replenish the actin monomer pool and to generate uncapped barbed actin filament ends for new elongation. We propose that Ssh monitors the level of actin filaments throughout this morphological response. At early stages, before significant levels of new actin filaments have been formed, low-level Ssh activity will act in opposition to LIMK to maintain a limited pool of active cofilin sufficient to remodel the existing actin filament network. Later, as new actin filaments accumulate and the PI3K signal declines at between 30 and 60 minutes after insulin stimulation, Ssh activity will come to dominate through its association with actin filaments and, perhaps, through inhibition of LIMK (Soosairajah et al., 2005). This will reduce cofilin phosphorylation increasing the level of actin depolymerisation to restore the F-actin:G-actin equilibrium. This dynamic regulation, we suggest, helps the cell to generate the robust but self-limiting actin filament response to acute actin signalling. In the context of a graded extracellular signal in the developing embryo (Wood et al., 2006), a similar system could act over spatially distinct regions of the cell to facilitate chemotaxis by coordinating the polymerisation of actin filaments at the cell front, with their disassembly at the cell rear.

## Materials and Methods
### Cell culture methods
S2R$^+$ and Kc167 cells were maintained in Schneider's *Drosophila* medium (Invitrogen) supplemented with 10% (v/v) heat-inactivated foetal calf serum (FCS) (Helena Biosciences) and antibiotics (50 units/ml penicillin and 50 μg/ml streptomycin; both from Sigma) in T25 flasks (Falcon, BD Biosciences) at 24°C. For passage of S2R$^+$ cells, cells were removed from culture flasks using trypsin-EDTA (Invitrogen). To determine the effect of insulin on PI3K signalling including actin reorganisation, cells were grown in serum-free medium overnight and then treated with bovine insulin (10 μg/ml; Sigma) for different times. Other growth factors used in this study were human EGF at 200 ng/ml (R&D Systems), murine VEGF at 50 ng/ml and human PDGF-BB at 125 ng/ml (both from PeproTech Inc.). For inhibitor treatments, cells were treated with 100 nM wortmannin (Calbiochem), 10-100 μM LY294002 (Calbiochem), 1 μg/ml latrunculin B (Calbiochem), 1 μg/ml jasplakinolide (Invitrogen) or 2 μg/ml cytochalasin D (Sigma). All inhibitors were made up in DMSO, which served as a vehicle-alone control.

### dsRNA production and RNAi
Primer sequences of ~21 bp (supplementary material Table S2) flanked with T7 sites, were chosen to PCR amplify ~500-1500 bp of exonic sequences of the genes to be silenced. PCR was carried out using HotStarTaq DNA polymerase (Qiagen).

PCR amplification was confirmed by 1% agarose gel electrophoresis using the GeneRuler 1-kb marker to assess the size of PCR products. dsRNAs were generated from PCR products by in vitro transcription using the MEGAscript™ High Yield Transcription Kit (Ambion). Reactions were conducted at 37°C overnight and dsRNAs were purified using Multiscreen PCR$_{96}$ purification plates (Millipore) attached to a vacuum pump. Purified dsRNAs were re-suspended in TE buffer (10 mM Tris-HCl pH 8.0, 1 mM EDTA) and annealed at 95°C for 15 minutes followed by slow cooling to room temperature (RT). The dsRNA concentration was estimated on 1% agarose gels using 500 ng of the GeneRuler 1-kb marker and dsRNAs were stored at –20°C until used. For dsRNA treatment, S2R$^+$ cells were typically suspended at $2×10^6$ cells/ml in Schneider's serum-free medium and 300 µl of cells per well were plated into 6-well tissue culture plates (Falcon, BD Biosciences). dsRNA was added directly to the medium to a final concentration of 0.3 µM, followed by gentle agitation. Cells were incubated for 30 minutes at RT followed by addition of 1 ml of Schneider's medium supplemented with 10% FCS. For proteomic experiments, each dsRNA treatment was conducted in triplicate on separate days. To allow turnover of target proteins cells were incubated for 5 days prior to harvesting for analysis.

## Sample preparation for 1D and 2D SDS-PAGE

Cells were washed gently with ice-cold PBS and lysed in NP40 lysis buffer (50 mM HEPES, 150 mM NaCl, 1% NP40, 1 mM EDTA) or 2D lysis buffer (8 M urea, 2 M thiourea, 4% CHAPS, 1 mM EDTA, 10 mM Tris-HCl pH 8.3), both supplemented with protease inhibitors (17 µg/ml aprotinin; 1 µg/ml pepstatin; 1 µg/ml leupeptin, 100 µg/ml AEBSF) and phosphatase inhibitors (2 mM sodium orthovanadate, 5 µg/ml BpVphen, 5 µM fenvalerate, 1 µM okadaic acid). For 1D SDS-PAGE, cells were lysed in NP40 lysis buffer and scraped off on ice. Cells lysed in 2D lysis buffer were homogenised by passage (six times) through a 25G needle. Insoluble material was removed by centrifugation (13,000 rpm for 10 minutes at 4°C). Protein concentrations were determined using Coomassie Protein Assay Reagent (Pierce) and a bovine serum albumin (BSA) standard curve with three replicate assays performed per sample. For 1D SDS-PAGE, lysates were denatured in Laemmli sample buffer [50 mM Tris-HCl pH 6.8, 10% (v/v) glycerol, 2% (w/v) SDS, 0.1% (w/v) Bromophenol Blue, 2% (v/v) β-mercaptoethanol] and heated at 100°C for 5 minutes. 1D SDS-PAGE was performed following standard procedures.

## Fluorescence 2D-DIGE protein expression profiling

The N-hydroxy-succinimidyl (NHS) ester of Cy2 was purchased from GE Healthcare, whereas NHS-Cy3 and Cy5 were synthesized in-house following the protocol outlined in Chan et al. (Chan et al., 2005). 2D difference gel electrophoresis (2D-DIGE) was carried out in a dedicated clean-room essentially as described (Weeks et al., 2006). For this, 120 µg of protein extract from each triplicate sample was labelled with NHS-Cy3 or NHS-Cy5 at 4 pmol dye/µg protein on ice in the dark for 30 minutes. Equal amounts of protein extract from each experiment were pooled together and labelled with NHS-Cy2 to create an internal standard which was run on all gels against the Cy3- and Cy5-labelled samples to aid in spot matching and quantification (Gharbi et al., 2002). Labelling reactions were quenched with a 20-fold molar excess of free L-lysine to dye and differentially labelled samples mixed appropriately. Final volumes were adjusted to 450 µl with 2D lysis buffer with final concentrations of 65 mM DTT, 2% carrier Ampholine/ Pharmalytes (50:50 v/v) pH 3-10 and 0.05% Bromophenol Blue. For 2D SDS-PAGE, 24-cm, non-linear pH 3-10 IPG strips (GE Healthcare) were rehydrated with Cy-labelled samples overnight in the dark at RT prior to isoelectric focusing on a Multiphor II apparatus (GE Healthcare) for 80 kVh at 18°C. Strips were then incubated for 10 minutes in equilibration buffer (50 mM Tris-HCl pH 6.8, 6 M (w/v) urea, 30% (v/v) glycerol, 2% (w/v) SDS) containing 65 mM DTT, and then for 10 minutes in the same buffer containing 240 mM iodoacetamide. IPG strips were transferred onto 1.5-mm thick 24×20 cm 12% polyacrylamide gels cast between low-fluorescence glass plates and bonded to the inner surface of one plate with bind-silane (PlusOne, GE Healthcare). Strips were overlaid with 0.5% (w/v) low-melting point agarose in Tris-glycine-SDS electrophoresis buffer (Severn Biotech) with Bromophenol Blue. Gels were run at 2 W per gel at 8°C in an Ettan 12 apparatus (GE Healthcare) until the dye front had run off and were then scanned (between plates) on a Typhoon 9400 multicolour fluorescence imager using ImageQuant software (GE Healthcare). Images were imported into DeCyder™ image analysis software (GE Healthcare) for comparison of sample feature volumes with the corresponding internal standard feature volumes giving a standardised abundance for each matched gel feature. Standardised abundances were then averaged from the triplicates for each experimental condition and features found on all images were selected for MS-based identification if they displayed a ⩾1.5-fold average change in abundance versus the untreated control with $P⩽0.05$ (Student's $t$-test). Proteins were then visualised by staining of gels with colloidal Coomassie Brilliant Blue and the gels were imaged and matched to the corresponding Cy-dye images using DeCyder software essentially as described (Chan et al., 2005). From this, a list of coordinates of spots of interest was generated for automated spot excision using an Ettan spot-picking robot (GE Healthcare).

## Protein identification by mass spectrometry

In-gel tryptic digestion of excised gel pieces was performed as previously described (Weeks et al., 2006). For peptide mass fingerprinting, 0.5 µl of tryptic digest was mixed with 1 µl of matrix – saturated aqueous 2,5-dihydroxybenzoic acid (DHB) – and spotted onto a sample target and dried. Matrix-assisted laser desorption/ionization time-of-flight (MALDI-TOF) mass spectra were acquired using an externally calibrated Ultraflex mass spectrometer (Bruker Daltonics) in the reflector mode. After internal calibration using trypsin autolysis peaks, prominent peaks in the mass range m/z 500-5000 were used to generate a peptide mass fingerprint which was searched against the updated NCBI database using Mascot version 2.0.02 (Matrix Sciences). Identifications were accepted when a minimum of six peptide masses matched a particular protein (mass error of ±100 ppm, allowing one missed cleavage), sequence coverage was >25%, MOWSE scores were higher than a threshold value of $P=0.05$, the predicted protein mass agreed with the gel-based mass and *Drosophila* sequences were identified. Identifications were also made by peptide sequencing using nano-liquid chromatography-electrospray ionization collision-induced dissociation tandem mass spectrometry (LC-MS/MS). This was performed on an Ultimate HPLC (Dionex) with a PepMap C18 75 µm inner-diameter column (LC Packings) at a flow rate of 300 nl/minutes, coupled to a Quadrupole Time-Of-Flight 1 (QTOF1) mass spectrometer (Waters/Micromass, Manchester, UK). Spectra were processed using MassLynx software (Waters) and submitted to Mascot database search routines. Positive identifications were accepted when at least two peptide sequences matched an entry with MOWSE scores above the $P=0.05$ threshold value.

## Phosphopeptide analysis using TiO$_2$ micro-columns and LC-MS/MS

Enrichment of phosphorylated peptides from peptides generated by in-gel digestion of selected protein spots was performed using TiO$_2$ essentially as described in (Larsen et al., 2005). Briefly, ~3-mm-long TiO$_2$ micro-columns were packed in GELoader tips with a small C8 3M Empore plug. The trypsin digests from the two cofilin protein spots were diluted into 5% TFA, 80% acetonitrile (with inclusion of 50 mg/ml phthalic acid) and loaded onto the TiO$_2$ micro-columns. The columns were washed with 5% TFA, 80% acetonitrile and bound phosphorylated peptides were eluted with 15 µl ammonia solution [10 µl ammonia (25% solution) in 490 µl water]. Eluates were acidified and analyzed by MALDI-TOF MS and LC-MS/MS. MALDI-TOF MS was performed on a Voyager STR mass spectrometer (PerSeptive Biosystems, Framingham, MA). All spectra were obtained in the positive reflector mode and DHB (20 g/l) in 50% acetonitrile, 1% phosphoric acid was used as the matrix. Data analysis was performed using MoverZ software (www.proteometrics.com) and peptide assignment was accomplished using GPMAW software (welcome.to/gpmaw). LC-MS/MS was performed on a Proxeon Biosystem Easy-nLC nanoflow system (Proxeon Biosystems, Odense, Denmark) coupled to a QTOF Ultima mass spectrometer (Waters/Micromass, Manchester, UK). Peptides were loaded onto a 75 µm inner-diameter fused silica pre-column (ReproSil–Pur, Germany) and eluted with a 1.5% gradient (buffer A: 0.5 % acetic acid; buffer B: 0.5% acetic acid in 80% acetonitrile) onto a 50 µm inner-diameter fused silica analytical column (ReproSil-Pur) and into the mass spectrometer. The mass spectrometer was operated in data-dependent acquisition mode and two of the most intense ions were selected for collision-induced dissociation per MS scan. The data were processed using MassLynx software and pkl files were searched using an in-house version of Mascot.

## Immunoblotting and immunofluorescence staining

Extracts separated by 1D or 2D SDS-PAGE were blotted onto Immobilon P membrane (Millipore) and blocked with 5% (w/v) BSA in TBS-T [50 mM Tris pH 8.0, 150 mM NaCl, 0.1% (v/v) Tween-20]. Membranes were probed with antibodies against C-terminal *Drosophila* Akt, *P*-Akt (both from S. Leevers, CRUK), *P*-S6K (Cell Signalling Technology), *PP*-ERK (Sigma), β-actin (Sigma) or *P*-cofilin (against the peptide acetyl-ApSGVTVSDC, Eurogentec). Membranes were washed (three times 10 minutes) in TBS-T, incubated with the appropriate horseradish-peroxidase-conjugated secondary antibody (Amersham Pharmacia), washed again and developed using enhanced chemiluminescence (PerkinElmer, Inc.). For immunostaining, cells were washed with PBS and fixed with 4% (v/v) formaldehyde in PBS for 10 minutes. After washing with PBS, cells were permeabilised with 0.1% (v/v) Triton X-100 in PBS for 5 minutes, washed again and blocked with 5% (w/v) BSA in PBS for 1 hour. For *P*-Akt staining, cells were incubated with primary antibody (1:300 in PBS) overnight at 4°C, followed by incubation with secondary anti-rabbit antibody conjugated to Cy5 for 1 hour at RT. For actin, tubulin and DNA staining, the fixed and permeabilised cells were incubated for 1 hour at RT with Rhodamine-phalloidin (1:1000), FITC-conjugated anti-tubulin antibody (1:1000) and DAPI (1:2000) respectively, all diluted in PBS. Fluorescent images were acquired using a Nikon 2000E microscope with 20× and 40× objectives fitted with a cooled CCD camera (Cool Snap; Roper) and using MetaMorph software (Universal Imaging Inc.). Within each experiment, all images were acquired and processed in an identical fashion to enable comparison across the image series.

## Time-lapse microscopy

Phase-contrast and fluorescence time-lapse movies were taken on a Nikon 2000E microscope with a 100× oil immersion lens at 20-second intervals. Actin dynamics were analysed in live dsRNA-treated cells by time-lapse fluorescence microscopy using GFP-moesin to visualise F-actin. For this, cells were treated for 4 days with dsRNAs and then plated onto uncoated glass dishes. Baculovirus harbouring DNA driving the expression of the actin-binding region of moesin fused to GFP from the actin5c promoter was then added to the cells and incubated overnight. Actin reorganisation in the cells was filmed from 3 minutes before until 10 minutes after addition of 10 μg/ml insulin. Kymographs were generated from time-lapse movie images using MetaMorph software. For this, five to ten 1-pixel-thick lines were drawn across the cell edges of one to three cells in the field and the pixel intensities along each line combined to generate the kymographs. Representative cells, lines and kymographs are shown for each experiment.

## References

**Arber, S., Barbayannis, F. A., Hanser, H., Schneider, C., Stanyon, C. A., Bernard, O. and Caroni, P.** (1998). Regulation of actin dynamics through phosphorylation of cofilin by LIM-kinase. *Nature* **393**, 805-809.

**Bamburg, J. R.** (1999). Proteins of the ADF/cofilin family: essential regulators of actin dynamics. *Annu. Rev. Cell. Dev. Biol.* **15**, 185-230.

**Benard, V., Bohl, B. P. and Bokoch, G. M.** (1999). Characterization of rac and cdc42 activation in chemoattractant-stimulated human neutrophils using a novel assay for active GTPases. *J. Biol. Chem.* **274**, 13198-13204.

**Biyasheva, A., Svitkina, T., Kunda, P., Baum, B. and Borisy, G.** (2004). Cascade pathway of filopodia formation downstream of SCAR. *J. Cell Sci.* **117**, 837-848.

**Bubb, M. R., Senderowicz, A. M., Sausville, E. A., Duncan, K. L. and Korn, E. D.** (1994). Jasplakinolide, a cytotoxic natural product, induces actin polymerization and competitively inhibits the binding of phalloidin to F-actin. *J. Biol. Chem.* **269**, 14869-14871.

**Carlier, M. F., Laurent, V., Santolini, J., Melki, R., Didry, D., Xia, G. X., Hong, Y., Chua, N. H. and Pantaloni, D.** (1997). Actin depolymerizing factor (ADF/cofilin) enhances the rate of filament turnover: implication in actin-based motility. *J. Cell Biol.* **136**, 1307-1322.

**Chan, H. L., Gharbi, S., Gaffney, P. R., Cramer, R., Waterfield, M. D. and Timms, J. F.** (2005). Proteomic analysis of redox- and ErbB2-dependent changes in mammary luminal epithelial cells using cysteine- and lysine-labelling two-dimensional difference gel electrophoresis. *Proteomics* **5**, 2908-2926.

**de Graauw, M., Tijdens, I., Cramer, R., Corless, S., Timms, J. F. and van de Water, B.** (2005). Heat shock protein 27 is the major differentially phosphorylated protein involved in renal epithelial cellular stress response and controls focal adhesion organization and apoptosis. *J. Biol. Chem.* **280**, 29885-29898.

**Firtel, R. A. and Chung, C. Y.** (2000). The molecular genetics of chemotaxis: sensing and responding to chemoattractant gradients. *Bioessays* **22**, 603-615.

**Gharbi, S., Gaffney, P., Yang, A., Zvelebil, M. J., Cramer, R., Waterfield, M. D. and Timms, J. F.** (2002). Evaluation of two-dimensional differential gel electrophoresis for proteomic expression analysis of a model breast cancer cell system. *Mol. Cell. Proteomics* **1**, 91-98.

**Ghosh, M., Song, X., Mouneimne, G., Sidani, M., Lawrence, D. S. and Condeelis, J. S.** (2004). Cofilin promotes actin polymerization and defines the direction of cell motility. *Science* **304**, 743-746.

**Hawkins, P. T., Eguinoa, A., Qiu, R. G., Stokoe, D., Cooke, F. T., Walters, R., Wennstrom, S., Claesson-Welsh, L., Evans, T., Symons, M. et al.** (1995). PDGF stimulates an increase in GTP-Rac via activation of phosphoinositide 3-kinase. *Curr. Biol.* **5**, 393-403.

**Hensbergen, P., Alewijnse, A., Kempenaar, J., van der Schors, R. C., Balog, C. A., Deelder, A., Beumer, G., Ponec, M. and Tensen, C. P.** (2005). Proteomic profiling identifies an UV-induced activation of cofilin-1 and destrin in human epidermis. *J. Invest. Dermatol.* **124**, 818-824.

**Hotulainen, P., Paunola, E., Vartiainen, M. K. and Lappalainen, P.** (2005). Actin-depolymerizing factor and cofilin-1 play overlapping roles in promoting rapid F-actin depolymerization in mammalian nonmuscle cells. *Mol. Biol. Cell* **16**, 649-664.

**Ibarra, N., Pollitt, A. and Insall, R. H.** (2005). Regulation of actin assembly by SCAR/WAVE proteins. *Biochem. Soc. Trans.* **33**, 1243-1246.

**Katso, R., Okkenhaug, K., Ahmadi, K., White, S., Timms, J. and Waterfield, M. D.** (2001). Cellular function of phosphoinositide 3-kinases: implications for development, homeostasis, and cancer. *Annu. Rev. Cell. Dev. Biol.* **17**, 615-675.

**Kiger, A., Baum, B., Jones, S., Jones, M., Coulson, A., Echeverri, C. and Perrimon, N.** (2003). A functional genomic analysis of cell morphology using RNA interference. *J. Biol.* **2**, 27.

**Kotani, K., Hara, K., Kotani, K., Yonezawa, K. and Kasuga, M.** (1995). Phosphoinositide 3-kinase as an upstream regulator of the small GTP-binding protein Rac in the insulin signaling of membrane ruffling. *Biochem. Biophys. Res. Commun.* **208**, 985-990.

**Kunda, P., Craig, G., Dominguez, V. and Baum, B.** (2003). Abi, Sra1, and Kette control the stability and localization of SCAR/WAVE to regulate the formation of actin-based protrusions. *Curr Biol* **13**, 1867-1875.

**Larsen, M. R., Thingholm, T. E., Jensen, O. N., Roepstorff, P. and Jorgensen, T. J.** (2005). Highly selective enrichment of phosphorylated peptides from peptide mixtures using titanium dioxide microcolumns. *Mol. Cell. Proteomics* **4**, 873-886.

**Lizcano, J. M., Alrubaie, S., Kieloch, A., Deak, M., Leevers, S. J. and Alessi, D. R.** (2003). Insulin-induced Drosophila S6 kinase activation requires phosphoinositide 3-kinase and protein kinase B. *Biochem. J.* **374**, 297-306.

**Mouneimne, G., Soon, L., DesMarais, V., Sidani, M., Song, X., Yip, S. C., Ghosh, M., Eddy, R., Backer, J. M. and Condeelis, J.** (2004). Phospholipase C and cofilin are required for carcinoma cell directionality in response to EGF stimulation. *J. Cell Biol.* **166**, 697-708.

**Nagata-Ohashi, K., Ohta, Y., Goto, K., Chiba, S., Mori, R., Nishita, M., Ohashi, K., Kousaka, K., Iwamatsu, A., Niwa, R. et al.** (2004). A pathway of neuregulin-induced activation of cofilin-phosphatase Slingshot and cofilin in lamellipodia. *J. Cell Biol.* **165**, 465-471.

**Nishita, M., Wang, Y., Tomizawa, C., Suzuki, A., Niwa, R., Uemura, T. and Mizuno, K.** (2004). Phosphoinositide 3-kinase-mediated activation of cofilin phosphatase Slingshot and its role for insulin-induced membrane protrusion. *J. Biol. Chem.* **279**, 7193-7198.

**Nishita, M., Tomizawa, C., Yamamoto, M., Horita, Y., Ohashi, K. and Mizuno, K.** (2005). Spatial and temporal regulation of cofilin activity by LIM kinase and Slingshot is critical for directional cell migration. *J. Cell Biol.* **171**, 349-359.

**Niwa, R., Nagata-Ohashi, K., Takeichi, M., Mizuno, K. and Uemura, T.** (2002). Control of actin reorganization by Slingshot, a family of phosphatases that dephosphorylate ADF/cofilin. *Cell* **108**, 233-246.

**Reif, K., Nobes, C. D., Thomas, G., Hall, A. and Cantrell, D. A.** (1996). Phosphatidylinositol 3-kinase signals activate a selective subset of Rac/Rho-dependent effector pathways. *Curr. Biol.* **6**, 1445-1455.

**Ridley, A. J., Schwartz, M. A., Burridge, K., Firtel, R. A., Ginsberg, M. H., Borisy, G., Parsons, J. T. and Horwitz, A. R.** (2003). Cell migration: integrating signals from front to back. *Science* **302**, 1704-1709.

**Song, X., Chen, X., Yamaguchi, H., Mouneimne, G., Condeelis, J. S. and Eddy, R. J.** (2006). Initiation of cofilin activity in response to EGF is uncoupled from cofilin phosphorylation and dephosphorylation in carcinoma cells. *J. Cell Sci.* **119**, 2871-2881.

**Soosairajah, J., Maiti, S., Wiggan, O., Sarmiere, P., Moussi, N., Sarcevic, B., Sampath, R., Bamburg, J. R. and Bernard, O.** (2005). Interplay between components of a novel LIM kinase-slingshot phosphatase complex regulates cofilin. *EMBO J.* **24**, 473-486.

**Tanaka, K., Okubo, Y. and Abe, H.** (2005). Involvement of slingshot in the Rho-mediated dephosphorylation of ADF/cofilin during Xenopus cleavage. *Zoolog. Sci.* **22**, 971-984.

**Vanhaesebroeck, B., Leevers, S. J., Ahmadi, K., Timms, J., Katso, R., Driscoll, P. C., Woscholski, R., Parker, P. J. and Waterfield, M. D.** (2001). Synthesis and function of 3-phosphorylated inositol lipids. *Annu. Rev. Biochem.* **70**, 535-602.

**Vartiainen, M. K. and Machesky, L. M.** (2004). The WASP-Arp2/3 pathway: genetic insights. *Curr. Opin. Cell Biol.* **16**, 174-181.

**Weeks, M. E., Sinclair, J., Butt, A., Chung, Y. L., Worthington, J. L., Wilkinson, C. R., Griffiths, J., Jones, N., Waterfield, M. D. and Timms, J. F.** (2006). A parallel proteomic and metabolomic analysis of the hydrogen peroxide- and Sty1p-dependent stress response in Schizosaccharomyces pombe. *Proteomics* **6**, 2772-2796.

**Wood, W., Faria, C. and Jacinto, A.** (2006). Distinct mechanisms regulate hemocyte chemotaxis during development and wound healing in Drosophila melanogaster. *J. Cell Biol.* **173**, 405-416.

**Yamamoto, M., Nagata-Ohashi, K., Ohta, Y., Ohashi, K. and Mizuno, K.** (2006). Identification of multiple actin-binding sites in cofilin-phosphatase Slingshot-1L. *FEBS Lett.* **580**, 1789-1794.

**Yanagawa, S., Lee, J. S. and Ishimoto, A.** (1998). Identification and characterization of a novel line of Drosophila Schneider S2 cells that respond to wingless signaling. *J. Biol. Chem.* **273**, 32353-32359.

**Yang, N., Higuchi, O., Ohashi, K., Nagata, K., Wada, A., Kangawa, K., Nishida, E. and Mizuno, K.** (1998). Cofilin phosphorylation by LIM-kinase 1 and its role in Rac-mediated actin reorganization. *Nature* **393**, 809-812.